Robust and Efficient Ridge-Based Palmprint Matching

Jifeng Dai, Jianjiang Feng, *Member*, *IEEE*, and Jie Zhou, *Senior Member*, *IEEE*

Abstract—During the past decade, many efforts have been made to use palmprints as a biometric modality. However, most of the existing palmprint recognition systems are based on encoding and matching creases, which are not as reliable as ridges. This affects the use of palmprints in large-scale person identification applications where the biometric modality needs to be distinctive as well as insensitive to changes in age and skin conditions. Recently, several ridge-based palmprint matching algorithms have been proposed to fill the gap. Major contributions of these systems include reliable orientation field estimation in the presence of creases and the use of multiple features in matching, while the matching algorithms adopted in these systems simply follow the matching algorithms for fingerprints. However, palmprints differ from fingerprints in several aspects: 1) Palmprints are much larger and thus contain a large number of minutiae, 2) palms are more deformable than fingertips, and 3) the quality and discrimination power of different regions in palmprints vary significantly. As a result, these matchers are unable to appropriately handle the distortion and noise, despite heavy computational cost. Motivated by the matching strategies of human palmprint experts, we developed a novel palmprint recognition system. The main contributions are as follows: 1) Statistics of major features in palmprints are quantitatively studied, 2) a segment-based matching and fusion algorithm is proposed to deal with the skin distortion and the varying discrimination power of different palmprint regions, and 3) to reduce the computational complexity, an orientation field-based registration algorithm is designed for registering the palmprints into the same coordinate system before matching and a cascade filter is built to reject the nonmated gallery palmprints in early stage. The proposed matcher is tested by matching 840 query palmprints against a gallery set of 13,736 palmprints. Experimental results show that the proposed matcher outperforms the existing matchers a lot both in matching accuracy and speed.

Index Terms—Palmprint, orientation field, density map, data fusion, distortion, matching, cascade filtering, generalized Hough transform, naive Bayes classifier.

1 Introduction

The human palm consists of two main features: flexion creases and friction ridges [1]. Flexion creases are formed due to the folding of the palm. The three most salient flexion creases, termed major creases or principal lines [1], divide the palm into three regions: thenar, hypothenar, and interdigital (see Fig. 1). The palm also contains many minor creases, which are not as permanent as the major creases [1]. Friction ridges are formed as a result of a buckling instability in the basal cell layer of the fetal epidermis [2]. And an imaging resolution of about 500 ppi is required to observe the ridge feature. The patterns formed by the friction ridges on the palm are both unique and persistent, making it useful as a biometric trait for person identification. Law enforcement agencies throughout the world have been routinely collecting palmprints, together with fingerprints, from criminals since the early 20th century [3].

Existing research on palmprint recognition mainly concentrates on low-resolution palmprint images which can be acquired using cheap cameras [4], [5], [6], [7], [8], [9], [10], [11]. The images are usually captured in a contactless manner, and the resolution is about at 100 ppi. At such low resolution, ridges cannot be observed and matching is mainly based on major and minor creases. In [12], [13], [14], [15], researchers tried to explicitly extract and match major creases. In [5], [16], [17], [18], crease information is encoded and compared in various forms such as Gabor phase.

However, major biometric modalities used in large-scale person identification systems, such as forensic and border control systems, need to be both distinctive and insensitive to changes in age and skin condition. Thus, palmprint recognition systems for these applications have to be based on ridge features, although creases may be used as supplementary features. In fact, 500 ppi is the standard resolution for capturing palmprints in forensic applications [19] and person identification based only on ridge features (such as minutiae) is accepted in courts of law [1].

The literature of ridge-based palmprint recognition has still been very sparse until now. In [20], Jain and Feng proposed a minutiae-based palmprint recognition system achieving acceptable accuracy. In this system, a region growing algorithm was proposed to extract the ridge orientation in presence of creases and a novel minutia descriptor, MinutiaCode, was designed. In [21], a multi-feature-based palmprint recognition system was proposed by Dai and Zhou, where multiple features, including minutia points, orientation field, density map, and major creases, are extracted and compared to achieve higher accuracy.

Despite the available techniques, there are still some problems remaining to be solved for large-scale applications. Some of the most important problems are:

• *The authors are with the Department of Automation, Tsinghua University, Beijing 100084, China. E-mail: djf05@mails.tsinghua.edu.cn, {jfeng, jzhou}@tsinghua.edu.cn.*

Manuscript received 16 Apr. 2011; revised 15 Sept. 2011; accepted 29 Oct. 2011; published online 7 Dec. 2011.
Recommended for acceptance by S. Prabhakar.
For information on obtaining reprints of this article, please send e-mail to: tpami@computer.org, and reference IEEECS Log Number TPAMI-2011-04-0236.
Digital Object Identifier no. 10.1109/TPAMI.2011.237.

0162-8828/12/$31.00 © 2012 IEEE Published by the IEEE Computer Society

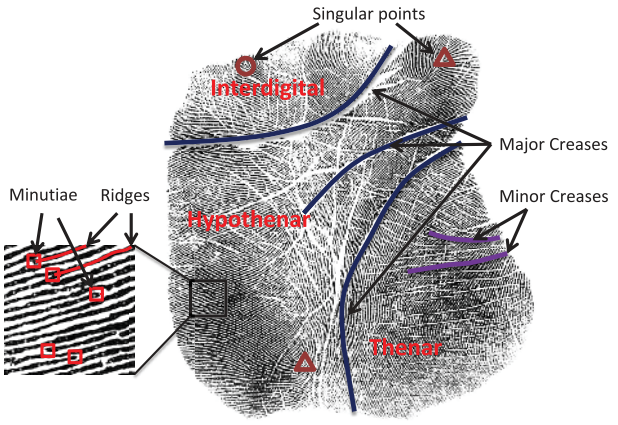

Fig. 1. Crease and ridge features in a palmprint.

1. Skin distortion. Unlike the finger tip, the palm contains many joints and its size is much larger. As a result, distortion is quite common between different impressions of the same palm and is much more serious than the distortion of fingerprints. Fig. 2 shows an example of palmprints with distortion. Since the algorithms in [20], [21] used a global rigid transformation model, they are fragile to large distortion.
2. Diversity of different palm regions. Different regions of palmprints have varying quality and distinctiveness. While the existing algorithms in [20], [21] treat the identifying information from the different regions of a palm equally, it is important to weight such information according to its quality and distinctiveness to have a reliable matching procedure.
3. Computational complexity. Because palmprints in operational palmprint databases are usually not positioned in a common coordinate system, minutiae matching algorithms have to try all possible rotation and translation or all possible correspondence of minutiae. Since palmprints contain much more minutiae than fingerprints, those matching algorithms which are basically adapted from fingerprint matching algorithms are very inefficient in matching palmprints. For example, a well-known commercial matcher, VeriFinger [22], can perform more than 15,000 fingerprint matches per second, but only three palmprint matches per second. The matching algorithms in [20], [21] are also very slow.

The limitations of the existing palmprint matching algorithms in [20], [21] can be summarized as that these algorithms are basically adapted from fingerprint matching algorithms [23], [24]. To develop an accurate and efficient palmprint matching algorithm, the intrinsic characteristics of palmprints have to be utilized.

Motivated by the matching strategies of human palmprint experts [1], [25], such as registering palmprints using clues from orientation field and rejecting nonmated palmprints based on partial region, we developed a novel palmprint matching system for 1:N matching. The main contributions include

1. A quantitative statistical study of various characteristics of palmprints is conducted to guide the design and parameter selection of the matching system.

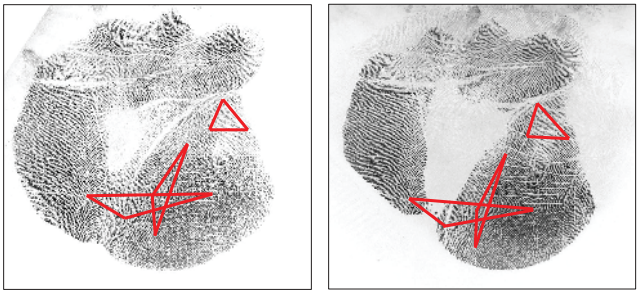

Fig. 2. A pair of mated palmprints with large distortion, as indicated by the corresponding triangles.

2. To deal with the distortion and the varying discrimination power of different palmprint regions, a segment-based palmprint matching and fusion algorithm is proposed. The whole palmprint image is divided into small segments, which are then separately matched to deal with distortion. The similarity between two palmprints is calculated by fusing the similarity scores of different segments using a Bayesian framework.
3. To reduce the computational complexity, an orientation field-based registration algorithm is designed for registering palmprints of different positions and rotations into the same coordinate system before matching. Furthermore, a cascade filter is built to reject nonmated gallery palmprints in an early stage by comparing just a small portion of the whole palmprint.

Experimental results of matching 840 query palmprints against a gallery set of 13,736 palmprints show that the proposed algorithm achieves large improvement in both matching accuracy and speed. In full-to-full palmprint matching experiments, a True Acceptance Rate (TAR) of 97.9 percent is obtained by the proposed algorithm when the False Acceptance Rate (FAR) is controlled at 2×10^{-7}. This TAR is 17 percent higher than that of the algorithm in [21] and 40 percent higher than that of the algorithm in [20]. In partial-to-full palmprint matching, the TAR is 91.9 percent at a FAR of 3×10^{-8}, 34 percent and 65 percent higher than the TARs of the algorithms in [21] and [20], respectively. Experimental results also show that the proposed algorithm can improve the palmprint matching speed by a factor of 132 compared with the algorithm in [21].

The rest of this paper is organized as follows: In Section 2, the statistics of palmprint characteristics is analyzed. Section 3 describes the proposed palmprint matching algorithm. In Section 4, the experimental results are presented and analyzed. Finally, we finish with conclusions in Section 5.

2 Statistical Analysis of Palmprints

While qualitative knowledge on palmprints is sufficient for human experts, in order to design an automatic system and optimize its parameters we need a quantitative study of palmprint features. In this section, the statistical characteristics of different palmprint features, different palmprint regions, as well as palmprint distortion are discussed.

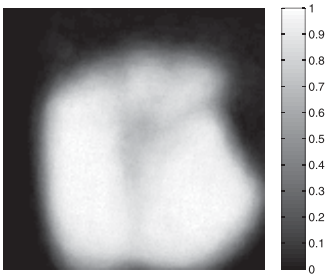

Fig. 3. Average palmprint region mask. The bright pixels correspond to the location that tends to be a valid palmar region.

2.1 Statistical Analysis of Different Features

The goal of a statistical study of palmprint features is to identify good features for registration and matching. A criterion is that the features with high consistency among different palms and low consistency among different regions of the same palmprint are useful for registering palmprints into the same coordinate system, while the features with high diversity among different palms are more important for matching.

To conduct a quantitative analysis of the features in palmprints, including orientation field and density map, we utilized 200 palmprints from 200 different palms. And they are composed of the first impressions of 40 different palms in the training set of the THUPALMLAB (see Table 3 for the details of this database) and another 160 palmprints further gathered from 160 palms. The palmprints are manually transformed into the same coordinate system, and those from the right hands are mirrored to increase the number of samples.

2.1.1 Region Mask

The region mask M of a palmprint I is a binary image where 1 indicates a valid palmar region. Region mask is estimated using the algorithm in [20]. As shown by the average palmprint region mask in Fig. 3, the central regions of about 50 percent palmprints are missing. This is very common in palmprints captured using contact-based techniques.

2.1.2 Orientation Field

The orientation field characterizes the ridge orientation at each location in the palmprint. To study its statistical characteristic, the palmprint is divided into nonoverlapped blocks of 64×64 pixels, and ridge orientation is estimated at each block using the algorithm in [20]. Let $\theta_i(x, y)$ denotes the orientation at (x, y) of the ith palmprint. We map it to a complex number of unit magnitude $z_i(x, y) = \cos(2\theta_i(x, y)) + j\ \sin(2\theta_i(x, y))$ for computational convenience. The mean of z_i at (x, y) is

$$\bar{z}(x, y) = \frac{\sum_{i \in T} z_i(x, y) M_i(x, y)}{\sum_{i \in T} M_i(x, y)}, \tag{1}$$

in which $M_i(x, y)$ is the region mask at (x, y) of the ith palmprint.

The average and the circular standard deviation values for the orientation field at (x, y) are calculated by [26]

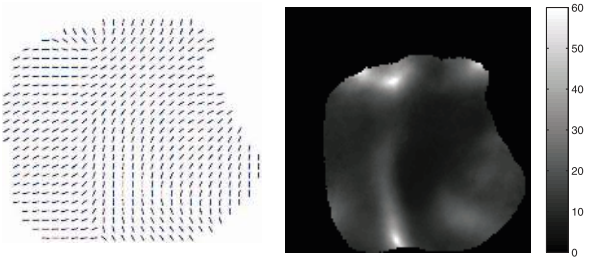

(a) (b)

Fig. 4. Statistical characteristics of orientation field: (a) and (b) are the mean and circular standard deviation for the orientation field, respectively. Note that bright pixels in (b) correspond to the location where singular points tend to appear.

$$\begin{cases} \bar{\theta}(x, y) = \frac{1}{2} Arg(\bar{z}(x, y)), \\ \sigma_\theta(x, y) = \frac{1}{2} \sqrt{-2 \ln \bar{z}(x, y)}. \end{cases} \tag{2}$$

The derived average and circular standard deviation images are shown in Figs. 4a and 4b. As shown in Fig. 4b, a large portion of the palmar region has low deviation, and the circular standard deviation is below 15 degrees in about 67 percent palmar region. This indicates there is a general ridge flow often repeated in the majority of the palmprints. Some common patterns in the orientation field of palmprints have been defined by palmprint experts [25], as shown in Fig. 5. In the thenar region, ridge flow forms a semicircular pattern around the thumb, which is termed "half-moon." In the hypothenar region, the characteristic is that ridges flow down and out of the hand. Near the top of the hypothenar region, ridges funnel toward the center. The ridges at the top side of the funnel are usually much flatter than those at the lower side. The orientation field shows a common pattern between different palms and has large variance in different regions of the same palmprint, making it a good feature for registering different palmprints.

2.1.3 Density Map

Density map depicts the ridge density of different locations in the palmar region. Density map is estimated by the algorithm in [21]. The average and standard deviation images of density map are shown in Figs. 6a and 6b, which are calculated by

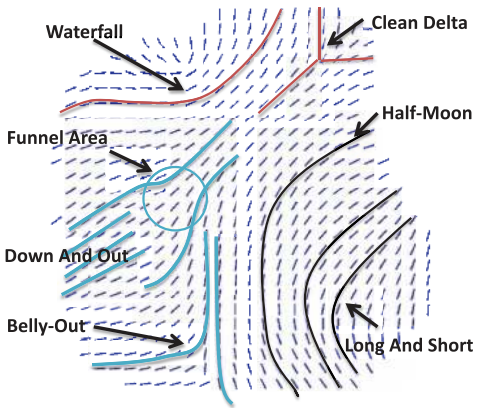

Fig. 5. Common ridge flow patterns in the average orientation field.

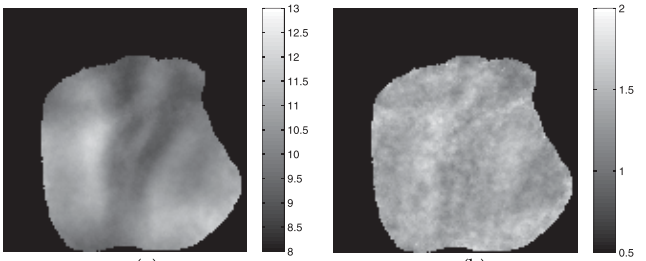

Fig. 6. Statistical characteristics of density map: (a) and (b) are the mean and standard deviation for the ridge distance, respectively.

$$\begin{cases} \bar{d}(x,y) = \frac{\sum_{i\in T} d_i(x,y) M_i(x,y)}{\sum_{i\in T} M_i(x,y)}, \\ \sigma_d(x,y) = \sqrt{\frac{\sum_{i\in T} [(d_i(x,y) - \bar{d}(x,y))^2 \cdot M_i(x,y)]}{\sum_{i\in T} M_i(x,y) - 1}}, \end{cases} \tag{3}$$

in which $d_i(x,y)$ is the ridge distance (reciprocal of ridge density) estimated at the 16×16 pixels block around (x,y) for the ith palmprint, $\bar{d}(x,y)$ and $\sigma_d(x,y)$ are the average and standard deviation values of the ridge distance at (x,y). As is shown in the statistical results, the average ridge distance scatters in the range of 8 to 12.5 pixels, while the standard deviation values are higher than 1.3 pixels in almost all the palmar region, showing low consistency among different palms.

2.2 Discrimination Power of Palmprint Features and Regions

Since ridge patterns in different palmar regions have different characteristics, the discrimination power of different regions also varies. In order to study this problem, a statistical experiment is conducted using the eight impressions of 40 different palms in the training set. All the palmprints are transformed into the same coordinate system manually. Next, the transformed palmprint images are divided into nonoverlapped blocks of 64×64 pixels to save computational cost. The discrimination power of the 510×510 pixel local region centered at each block is studied. The size is chosen so that there are sufficient features within to align successfully. When matching two palmprints, each block's local region is separately matched to the corresponding block's local region if they are valid palmprint regions. A total of 1,120 genuine matches and 101,280 impostor matches are performed using the algorithm in [21].

With the similarity scores of genuine and impostor match pairs from all the segments, the discrimination power of different features at different segments can be reflected by the True Acceptance Rate when the False Acceptance Rate is set as 10^{-4}, as shown in Fig. 7.

It can be seen from Fig. 7 that the discrimination power of different area varies significantly. The interdigital and the hypothenar regions show better discrimination power than the thenar region. This is because there are many creases in the thenar which significantly affect the extraction of ridge-based features. It is also shown that among the features of minutiae, orientation field, and density map, density map achieves the highest accuracy in most of the regions. Density map outperforms minutiae and orientation field in about 85 and 91 percent palmar regions, respectively, in the experiment. Some researchers have tried to apply it to fingerprint recognition but did not get a good result [27]. But this experiment proved that it is indeed a discriminating feature for palmprint recognition.

2.3 Distortion

The human hand has 27 bones, including the carpals in the wrist, the metacarpal bones running along the palm, and the phalanx bones in the fingers [28]. Due to the multiple degrees of freedom of the skeleton beneath the palm, distortion is very common in the palmar region. To study the distortion characteristic, a statistical experiment is conducted on the training set.

The registered palmprint images are divided into nonoverlapped blocks of 64×64 pixels as above. The distortion of the 510×510 pixel local region centered at each block is studied. The eight impressions of each palm are finely aligned with each other, generating 1,120 matching pairs in total. Each local region is aligned to the corresponding local region, respectively, using the generalized Hough transform (GHT)-based minutiae matching algorithm [23], and the displacement parameters for all the local regions are recorded. For a given matching pair, let $(\Delta x_k, \Delta y_k, \Delta\theta_k)$ denote the displacement parameters for the kth local region, then the mean displacement between two palmprints is calculated by

$$\begin{cases} \bar{\Delta x} = \frac{1}{N_a} \sum_{k=1}^{N_a} \Delta x_k, \\ \bar{\Delta y} = \frac{1}{N_a} \sum_{k=1}^{N_a} \Delta y_k, \\ \bar{\Delta\theta} = \frac{1}{2} atan\left(\sum_{k=1}^{N_a} \frac{\sin 2\Delta\theta_k}{\cos 2\Delta\theta_k} \right), \end{cases} \tag{4}$$

in which N_a is the number of corresponding local regions for the matching palmprint pair.

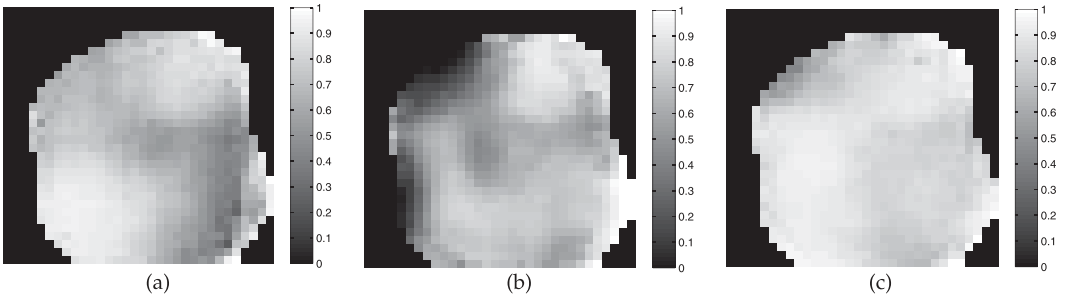

Fig. 7. TARs of three different features at different palmprint regions when the FAR is set as 10^{-4}: (a) minutiae, (b) orientation field, (c) density map.

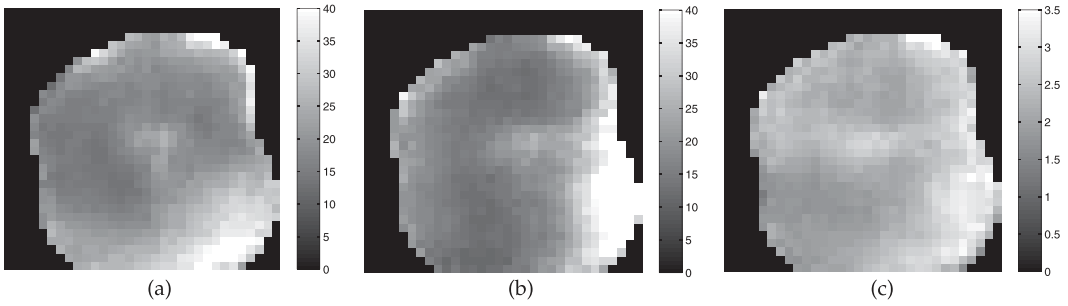

Fig. 8. Distortion characteristics of the palmprints: (a), (b), and (c) show the average absolute values of $\tilde{\Delta}x_k$, $\tilde{\Delta}y_k$, $\tilde{\Delta}\theta_k$, respectively. $\tilde{\Delta}x_k$ and $\tilde{\Delta}y_k$ are in pixels, while $\tilde{\Delta}\theta_k$ is in degrees.

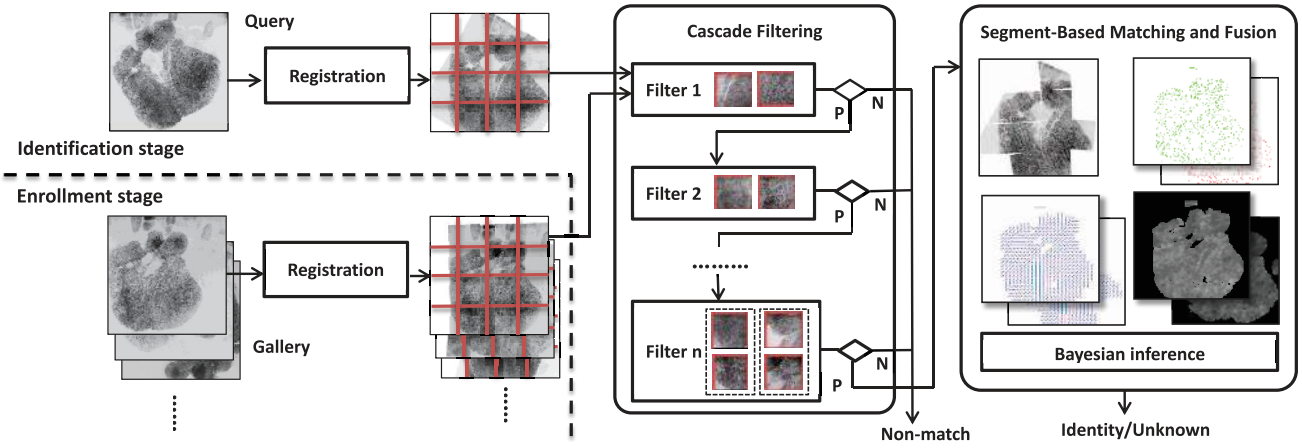

Fig. 9. Outline of the proposed palmprint identification system.

To characterize the distortion, the relative displacement $(\tilde{\Delta}x_k, \tilde{\Delta}y_k, \tilde{\Delta}\theta_k)$ for each local region is calculated by subtracting the mean displacement from $(\Delta x_k, \Delta y_k, \Delta\theta_k)$. Finally, the average of the absolute values for the relative displacement parameters in each local region are calculated using all the matching pairs.

The calculated average absolute values are shown in Fig. 8. As shown in the image, distortion widely exists in the palmprint images, especially at the thenar region. The adduction/abduction movement of the human thumb is controlled by its carpal-metacarpal joint at the thenar region which is highly flexible [29], leading to greater susceptibility of the thenar regions toward distortion. And the distortion of other regions still cannot be ignored. Due to the universality of distortion in palmprints, distortion tolerant algorithms are required to achieve high accuracy for large-scale applications.

2.4 Summary

Major conclusions pertaining to palmprint characteristics are summarized as follows:

1. Orientation field shows high consistency among the same region of different palms and low consistency among different regions of the same palmprint.
2. Different regions and different features of the palmprint have varying discrimination power.
3. Distortion widely exists in the palmprint images.

3 Proposed Palmprint Matching System

3.1 System Outline

Motivated by the matching strategies of human palmprint experts and based on our quantitative study of palmprint statistics, we design a novel palmprint matching system for 1:N matching. The outline of the proposed palmprint matching system is shown in Fig. 9. The system is composed of three modules: palmprint registration, segment-based matching and fusion, and cascade filtering. The relations between the three modules and the major characteristics of palmprints summarized in Section 2.4 are shown in Fig. 10.

Since different palmprints share a lot of common ridge flow patterns, orientation field is used for palmprint registration, which transforms palmprints of different rotations and displacements into the common coordinate

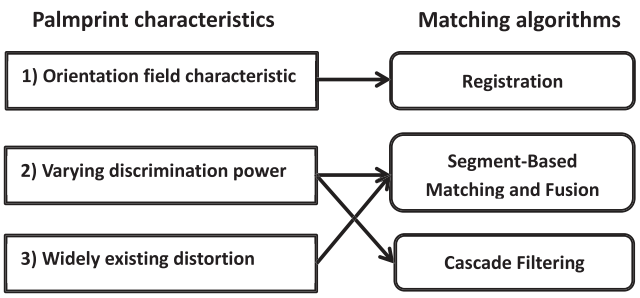

Fig. 10. Relations between the three characteristics of palmprints and the three modules of the proposed matching algorithm.

system. Thus, tight position constraint can be enforced in the matching algorithm, and matching speed can be greatly improved.

The segment-based matching and fusion algorithm is proposed to deal with distortion and varying discrimination power of different regions. Registered palmprints are divided into small segments. During palmprint matching, all the corresponding segments are finely aligned and compared, respectively. When distortion occurs, the segments will rotate and shift to compensate for the distortion. In this way, the influence of distortion can be effectively reduced. The similarity score is calculated at each segment for each feature, respectively, and the weights of various features at different segments are determined by learning.

As some segments in palmprints are very distinctive, it is possible to discard many nonmated gallery palmprints by just comparing these distinctive segments. The cascade filter is based on this idea.

In application, the proposed palmprint matching system operates as follows:

1. Palmprint registration is performed for the gallery palmprints in the enrollment stage and for the query palmprints in the identification stage separately. The gallery palmprints are generally full palmprints, while the query palmprints are live-scanned full palmprints from unknown suspects or latents recovered from crime scenes. The full palmprints are automatically registered by the proposed algorithm, while the latents are manually registered due to small palmar area, which is a common practice.[1]
2. Corresponding segments between the query and the gallery palmprints are compared sequentially based on an ordering determined by the cascade filter. Gallery palmprints which are very dissimilar to the query are rejected at once. Generally, a large portion of the gallery palmprints are rejected after comparing just a few segments.
3. After cascade filtering, the query palmprint is matched with the remaining gallery palmprints by the segment-based matching and fusion algorithm to determine the true mate of the query palmprint.

3.2 Registration

Palmprint images in law enforcement databases are generally not in the same coordinate system since they are usually captured without posture and position restriction. Registration is thus necessary to bring different palmprints into the same coordinate system to facilitate the matching. Registration is an indispensable step in most biometric recognition techniques, such as iris [31], face [32]. Iris is generally registered by its inner and outer circular contours, while face is generally registered by the location of eyes. The acceleration gained by registration is due to the tight position constraint in matching registered images. In case of minutiae matching, a minutia point in the query palmprint just needs to be matched with a small portion of the minutia points in the gallery palmprint whose location and direction are similar to it, reducing the computational complexity significantly.

1. The latents recovered from crime scenes are few and valuable. Palmprint experts usually manually mark the ridge features and determine the locations of latents based on the latent shape as well as some fine orientation field and crease features [25].

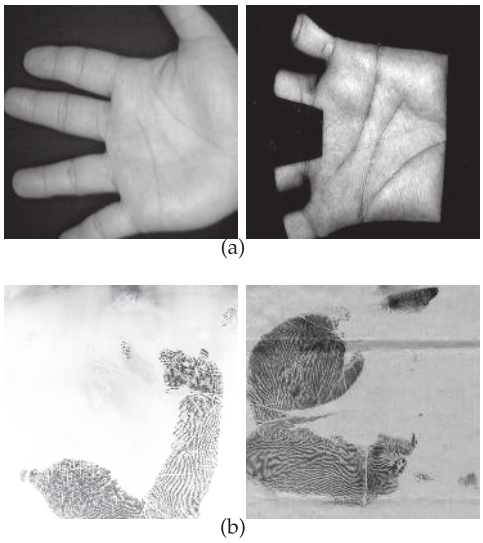

Fig. 11. Palmprint images captured (a) by contactless techniques in laboratory environment and (b) by contact-based techniques in operational environment. The left one in (a) is from the CASIA palmprint database [16] and the right one in (a) is from the PolyU palmprint database [30].

The key to registration is to find a good feature, which is similar between different palms, contains sufficient information to determine the correct position, and is robust to noise and incomplete impressions. Existing palmprint registration methods, which are based on intervals between fingers [4], [5], [33], [34], [35], hand contour [36], or principal lines [13], are mainly designed for contactless low-resolution palmprint verification systems. The low-resolution palmprints are captured by contactless devices, which ensures the whole palmar region and the finger roots are visible. However, in palmprints captured using contact-based techniques (such as inking and FTIR sensors, see Fig. 11), fingers are not available and principle lines and hand contours are usually incomplete or not reliable, making registration a challenging task. The statistical analysis in Section 2.1 shows that the orientation fields of different palms are quite similar and the orientation fields in different palmar regions are very distinctive, making orientation field a promising feature for palmprint registration.

Given the orientation field of an original (unregistered) palmprint, the registration algorithm first estimates the rigid transformation between the unregistered orientation field and the reference orientation field, and then registers the original palmprint with respect to the reference. The average orientation field shown in Fig. 4 is used as the reference orientation field for all the palmprints. And the unregistered orientation field is registered to both the reference orientation field (left palmprint) and the mirrored version (right palmprint). The unregistered palmprint is deemed left/right if it is more similar to the left/right reference. The algorithm in [20] is used to estimate orientation field on nonoverlapped large blocks (64×64 pixels) in order to suppress noise and reduce the computational complexity of the registration algorithm.

The orientation field of an unregistered palmprint can be viewed as a transformed and noisy version of the reference

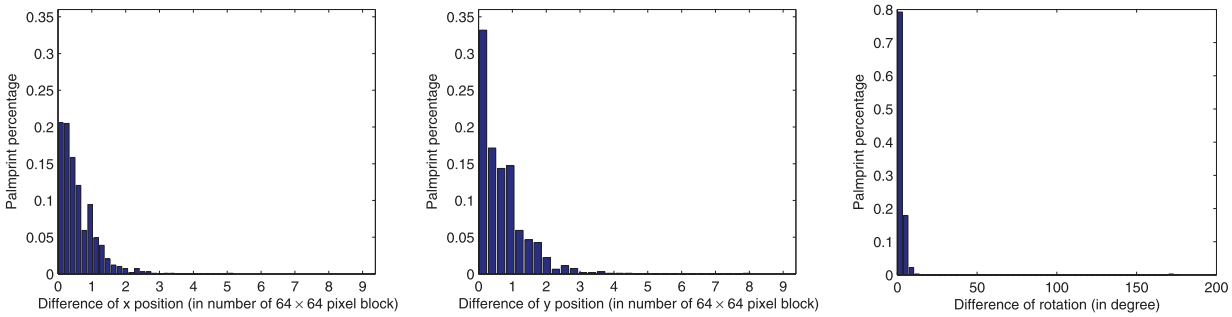

Fig. 12. Difference between the registration parameters estimated by the palmprint registration algorithm and the ground truth.

orientation field. The optimal rigid transformation between two orientation fields is found using the generalized Hough transform algorithm [37]. All possible pairs of blocks between the unregistered and reference orientation fields are considered to vote for the corresponding transformation parameters: rotation, horizontal, and vertical translation.

Since the features which are similar between different palms are important for registration, higher weights should be assigned to the votes from the regions with high orientation field consistence. Let $w(x, y)$ denote the weight for the vote given by (x, y) in the coordinate of reference orientation field, it is calculated by

$$w(x, y) = \frac{1}{1 + \sigma_\theta(x, y)}, \tag{5}$$

in which $\sigma_\theta(x, y)$ is the corresponding circular standard deviation of orientation field as defined in (2).

After all pairs of blocks are considered, the bin in the transformation space with the largest number of votes is chosen as the transformation parameter.

The palmprint registration algorithm is used to speed up matching with as small accuracy reduction as possible. Therefore, it is important to examine whether the different impressions of the same palmprint can be consistently transformed to the same coordinate system with small deviation. We conducted a systematic experiment to automatically evaluate the consistence of registration for different impressions of the same palmprint. Eight impressions of the 40 different palms in the training set of THUPALMLAB are used in this experiment. The ground truth transformation parameters between palmprints are first estimated using the minutiae matcher in [21] and then manually verified. Fig. 12 shows the histograms of the difference between the registration parameters estimated by the proposed registration algorithm and the ground truth. The vast majority of the palmprints can be successfully registered with small difference. The example in Fig. 13 shows that although the three different impressions of the same palmprint are quite different in direction and impression region, the registration results are very consistent. According to the histograms of registration consistence in Fig. 12, the maximum rotation and displacement allowed in matching are set as 20 degrees and five blocks of 64×64 pixels, respectively, in our experiments.

3.3 Segment-Based Matching and Fusion

As shown by the statistical results in Section 2, distortion usually occurs between palmprints, and the different features from different segments have large differences in discrimination power. Although some distortion models have been proposed for fingerprint [38], [39], [40], they are not suitable for palmprint because they are not efficient enough and the distortion of palmprints is much more serious. A segment-based matching and fusion algorithm is proposed to deal with the distortion and the varying discrimination power of different segments.

The registered palmprints are divided into 4×4 nonoverlapped segments of 510×510 pixels uniformly as in Fig. 9. The size is chosen so that there are sufficient features within each segment for successful minutiae matching, while the distortion within the segment is sufficiently small. Although there are numerous possible segmentation strategies, here we adopted this simple strategy to verify the effectiveness of our algorithm. The following procedures are performed at the segment level.

Each segment of 510×510 pixels from the query palmprint is matched with the corresponding segment from the gallery. Since the registration is coarse and may produce some deviations, the gallery segment is enlarged to 610×610 pixels to completely contain the query segment. So, the segments in the gallery palmprint are overlapped.

Before the matching is performed, first, the algorithm tests the completeness of the matching segments, which is measured by the foreground area size and the minimum minutiae number of the gallery and query segments within their overlapped palmprint region. In our algorithm, if the foreground area size is smaller than 76,800 pixels or the

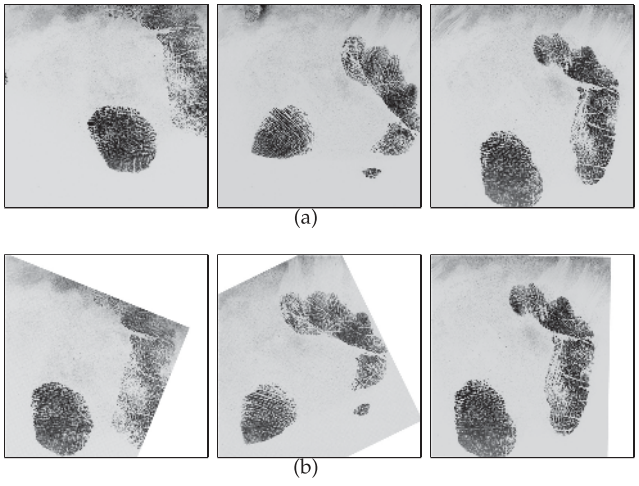

Fig. 13. Palmprints successfully registered by the proposed registration algorithm: (a) three original images from the same palm, (b) outputs of the registration algorithm.

TABLE 1
Notation in Feature Similarity Calculation

Notation	Meaning
S_m	Similarity score of minutiae
M	Number of matched minutiae.
M_E	Estimated minimal number of matched minutiae for the genuine.
M_q	Number of minutiae within the overlapped area for the query.
M_g	Number of minutiae within the overlapped area for the gallery.
S_o	Similarity score of orientation field.
N_o	Number of matched blocks where orientation field difference is within $22.5°$.
N_{o_E}	Estimated minimal number of blocks matched by orientation field for the genuine.
D_o	Mean of the orientation difference in all the blocks.
S_d	Similarity score of density map.
N_d	Number of matched blocks whose ridge distance difference is within 1 pixel.
N_{d_E}	Estimated minimal number of blocks matched by density map for the genuine.
N_b	Number of overlapped blocks between the matching segments.
$d_q(i)$	Ridge distance of the i^{th} query block.
$d_g(i)$	Ridge distance of the i^{th} gallery block.

minimum minutiae number is less than 20, then the matching segments are deemed to be very incomplete and are not considered.

Next, the remaining matching segments are finely aligned by the generalized Hough transform-based minutiae matching algorithm [41] with small tolerance. The maximum rotation and displacement allowed are set as 20 degrees and five blocks of 64×64 pixels, respectively. After a segment is aligned, the number of matched minutiae within it is counted, and the orientation field and density map are compared at blocks of 16×16 pixels using the equations in [42] and [21]. The notation used in feature similarity calculation is summarized in Table 1, and the similarity scores are calculated as

$$S_m = \frac{M}{M + M_E} \cdot \frac{M^2}{M_g M_q}, \tag{6}$$

$$S_o = \frac{N_o}{N_o + N_{o_E}} \cdot (1 - D_o/90°), \tag{7}$$

and

$$S_d = \frac{N_d}{N_d + N_{d_E}} \cdot \frac{1}{N_b} \sum_{i=1}^{N_b} \exp(-|d_g(i) - d_q(i)|), \tag{8}$$

in which M_E, N_{o_E}, and N_{d_E} are set as 5, 100, and 100, respectively.

After the above procedure, we get the similarity scores of three types of features for each segment. In addition, we observed that the consistence of the spatial transformations of segments can be used to distinguish genuine pairs from impostor ones, as shown in Fig. 14. The relative displacement described in Section 2.3 depicts the consistence and is used as the feature.

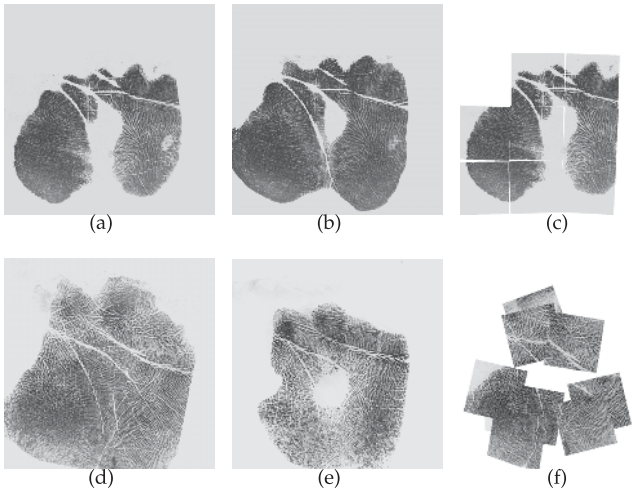

Fig. 14. Spatial transformations of segments for genuine and imposter match pairs: (a) and (b) are two different impressions of the same palm, (c) is the spatial transformations of aligning (a) to (b), (d) and (e) are the impressions of two different palms, (f) is the spatial transformations of aligning (d) to (e).

Finally, the relative displacement, the similarity scores of minutiae, orientation field, and density map are combined by Bayesian inference to output a match score. The probability that an observed palmprint match pair is genuine or impostor can be denoted by $P(Y|\{(\tilde{\Delta}x_k, \tilde{\Delta}y_k, \tilde{\Delta}\theta_k, S_{m_k}, S_{o_k}, S_{d_k})_{k=1,\ldots,16}\})$, in which $(\tilde{\Delta}x_k, \tilde{\Delta}y_k, \tilde{\Delta}\theta_k)$ denote the relative displacement parameters for the kth segment, S_{m_k}, S_{o_k}, and S_{d_k} are the segment's similarity scores of minutiae, orientation field and density map, respectively, Y can take two values: G (Genuine) or I (Impostor). The dimension of the feature vector of the whole palmprint is 96. To avoid the curse of dimensionality, the features are supposed to be independent. The likelihood ratio of genuine versus impostor can be decomposed as

$$\begin{aligned} L &= \frac{P(G|\{(\tilde{\Delta}x_k, \tilde{\Delta}y_k, \tilde{\Delta}\theta_k, S_{m_k}, S_{o_k}, S_{d_k})_k\})}{P(I|\{(\tilde{\Delta}x_k, \tilde{\Delta}y_k, \tilde{\Delta}\theta_k, S_{m_k}, S_{o_k}, S_{d_k})_k\})} \\ &= \frac{P(G)}{P(I)} \frac{P(\{(\tilde{\Delta}x_k, \tilde{\Delta}y_k, \tilde{\Delta}\theta_k, S_{m_k}, S_{o_k}, S_{d_k})_k\}|G)}{P(\{(\tilde{\Delta}x_k, \tilde{\Delta}y_k, \tilde{\Delta}\theta_k, S_{m_k}, S_{o_k}, S_{d_k})_k\}|I)} \\ &= \frac{P(G)}{P(I)} \prod_{k=1}^{16} \frac{P((\tilde{\Delta}x_k, \tilde{\Delta}y_k, \tilde{\Delta}\theta_k, S_{m_k}, S_{o_k}, S_{d_k})|G)}{P((\tilde{\Delta}x_k, \tilde{\Delta}y_k, \tilde{\Delta}\theta_k, S_{m_k}, S_{o_k}, S_{d_k})|I)} \\ &= \frac{P(G)}{P(I)} \prod_{k=1}^{16} \frac{P(\tilde{\Delta}x_k|G)P(\tilde{\Delta}y_k|G)P(\tilde{\Delta}\theta_k|G)}{P(\tilde{\Delta}x_k|I)P(\tilde{\Delta}y_k|I)P(\tilde{\Delta}\theta_k|I)} \\ &\quad \frac{P(S_{m_k}|G)P(S_{o_k}|G)P(S_{d_k}|G)}{P(S_{m_k}|I)P(S_{o_k}|I)P(S_{d_k}|I)} \\ &= \frac{P(G)}{P(I)} \prod_{k=1}^{16} L_k^s L_k^d, \end{aligned} \tag{9}$$

in which $\frac{P(G)}{P(I)}$ is the prior likelihood ratio, L_k^s and L_k^d are the likelihood ratio values estimated according to the similarity scores and displacement parameters of the kth segment, respectively. And the likelihood ratio values for the incomplete segments are set as 1.

To avoid the influence of very poor quality segments on genuine matches, a regularization term is added. So, the equation takes the form of

$$L = \frac{P(G)}{P(I)} \prod_{k=1}^{16} \left(\epsilon + L_k^s L_k^d\right), \tag{10}$$

where the regularization term ϵ is empirically set as 0.001.

In (9), $P(G)/P(I)$ is set as 1 and the PDFs are estimated using the results of matching the full palmprints from the training set. Gaussian Mixture Model (GMM) is used to approximate the 192 PDFs in (9). The Expected Maximization (EM) algorithm [43] is performed to search for the best fit between the models and the observed samples.

3.4 Cascade Filtering

Human experts can declare a pair of palmprints as unmatched as long as a portion of them is not matched [1]. The statistical result in Section 2.2 shows that some regions of the palmprint possess high discrimination power. Considering these facts, we develop a cascade filtering scheme to first compare these distinctive regions and quickly reject the dissimilar gallery palmprints. Cascade filtering is an important speedup technology in computer vision [44], [45], and multibiometrics [46]. Here, we first describe how the cascade filtering works and then present how to construct the cascade filters.

A cascade filter containing M filters can be denoted by $\mathbf{F} = \{(C_m, T_m)_{m=1,\ldots,M}\}$, in which C_m and T_m are the indices of the set of segments and the corresponding threshold used by the mth filter, respectively. In cascade filtering, a pair of palmprints passes through the filters sequentially. At the mth filter, the segments within C_m are matched, and the likelihood ratio is computed by

$$L_{C_m} = \frac{P(G)}{P(I)} \prod_{k \in C_m} \left(\epsilon + L_k^s\right). \tag{11}$$

The formula is different from (10) in that just the likelihood ratio terms estimated by the similarity scores within the segments of C_m are used since just the segments within C_m are available. If the calculated likelihood ratio, L_{C_m}, is lower than T_m, then the match pair is deemed unmatched and quickly dropped. Otherwise, it is passed to the next filter and the above procedure repeats. In this way, most nonmated gallery palmprints can be rejected by just comparing a small region of the whole palmprint, resulting in a significant reduction of computational cost.

To construct a cascade filter, which segments to use in each filter should be determined and appropriate thresholds should be chosen to exclude the nonmated palmprints while retaining the mated ones. Feature selection technique is brought in to determine the arrangements and parameters by viewing each segment as a feature. In most cases, the filter with more features can reject more nonmated pairs, while it takes more time to perform the filtering. To trade off between these two effects, our goal is to construct filters achieving desired True Rejection Rate (TRR) while keeping the False Rejection Rate (FRR) as 0 by using as few segments as possible. When building a filter, the possible combinations of segments form a search tree. The algorithm travels across this search tree in a breadth-first procedure. All possible filters using just one segment are first tested, and the best of them are selected. If the best one can reach the desired TRR, then the traversal procedure stops and the filter is built. Otherwise, all possible combinations of two segments are tested. The traversal procedure continues until the desired TRR cannot be achieved even using N_{max} segments. When a filter is built, it is added to the cascade filter. The segments used by the current filter are marked as occupied and the samples filtered are deleted. The algorithm tries to build the next filter with the left segments and training samples. So, the cascade filter building procedure is a combination of greedy algorithm and exhaustive strategy. When building a specific filter, the exhaustive strategy is utilized. Once a filter is found, it will not change in the following search procedure, which is greedy.

TABLE 2
Pseudocode of the Cascade Filter Construction Algorithm

```
Function ConstructCascadeFilter(L, Y)
//Input: L – likelihood ratios of all the segments in the
// training samples, Y – label array of the training samples
//Output: F – constructed cascade filter
do
  for number of segments to use, N, in 1 to N_max do
    generate combinations of N unoccupied segments {C_iN}
    foreach combination C_iN do
      [TRR_iN, T_iN]=ComputeTRRandThreshold(C_iN, L, Y)
    end
    find the filter (C_lN, T_lN) achieving the highest G_lN
    if TRR_lN > TRR_desire then
      add (C_lN, T_lN) to the cascade filter
      mark the segments in C_lN as occupied
      delete the samples filtered by (C_lN, T_lN) from L, Y
      break
    end
  end
while new filter is added
output the constructed cascade filter F = {(C_m, T_m)_m=1,...,M}
```

The pseudocode of the algorithm for cascade filter construction is shown in Table 2. The inputs are the likelihood ratios of all the segments in the training samples, L, and label array of the training samples, Y. In the algorithm of ComputeTRRandThreshold, the threshold, T_{i_N}, is set as the minimum likelihood ratio of the genuine match pairs and the corresponding TRR, TRR_{i_N}, is calculated.

4 Experiments

4.1 Palmprint Database

Till now, there has been no publicly available high-resolution palmprint database to our knowledge. To test the algorithm, we collected 1,280 palmprint images from 80 subjects (two palms per person and eight impressions per palm) using a commercial palmprint scanner of Hisign. To increase the size of the gallery, 13,616 different palmprints (one impression per palm) provided by a local police department are used as the background database. All these palmprints images are of $2{,}040 \times 2{,}040$ pixels and 500 ppi. The former set of 1,280 palmprints is termed a multi-impression subset and the latter is termed a uni-impression subset. As a whole, the database is termed the THUPALMLAB, and it contains 320 more palmprints than the former database used in [21]. The multiimpression subset of THUPALMLAB is available at http://ivg.au. tsinghua.edu.cn. To simulate the latent prints recovered from crime scenes, we created partial palmprints from different regions of the full palmprints. For each palm

TABLE 3
Summary of the THUPALMLAB Database

Print type		Number of palmprints	Number of palms
Multi-impression subset	Train	320	40
	Test	960	120
Uni-impression subset		13,616	13,616

in the multi-impression subset, seven partial images are cropped from the thenar, hypothenar, and interdigital regions of the last seven impressions, respectively. As a result, we obtain 160×21 partial palmprints from 160 different palms. Since the partial palmprints are cropped to simulate the latents, they are manually registered as in real applications. In experiments, the prints from the first 40 palms of the multi-impression subset are used for training, while the left prints are used for testing. Among all the palmprint images, about 20 percent of them are of relatively poor quality due to large amount of creases, deformation, smudges, blurs, incompleteness, etc. The database is summarized in Table 3.

4.2 Performance of Each Module

In this section, we evaluate the performance of each of the three modules, i.e., registration, segment-based matching and fusion, and cascade filtering.

4.2.1 Registration

To test the speedup gained by registration, the GHT-based minutiae matching algorithm is used to match different impressions of the same palm. The average time for the fine alignment is counted on the whole THUPALMLAB. Without registration, we cannot make assumptions about the relative position between the matching palmprints. The maximum rotation allowed is 360 degrees and the max displacement allowed is set as half of the palmprint image size. It takes about 5.1 seconds to match two full palmprints on average. When registration is performed, tight translation and rotation constraints can be applied. According to the histograms in Fig. 12, the maximum rotation and displacement allowed are set as 20 degrees and five blocks of 64×64 pixels, respectively. The average time cost of matching two full palmprints using the same minutiae matcher is reduced to 78 ms, which is about 65 times faster than without registration.

The computational cost of the registration procedure itself is composed of voting and best parameter searching, which are denoted by T_v and T_s. T_v is $O(N_u \times N_r)$ and T_s is $O(D \times D \times \Psi)$, where N_u and N_r are the numbers of nonoverlapped 64×64 foreground blocks in the unregistered and reference palmprints, respectively, D and Ψ are the maximum displacement and rotation allowed between the unregistered and reference palmprints. In experiments, T_v and T_s are about 900 for full palmprints, D and Ψ are set as half of the palmprint image size and 360 degrees, respectively. The execution time of the registration procedure is about 1.12 s in our experiment. Since it is performed in the enrollment stage for the gallery palmprints and in the identification stage for the query palmprint only once, its computational cost takes a very small portion of the online identification procedure.

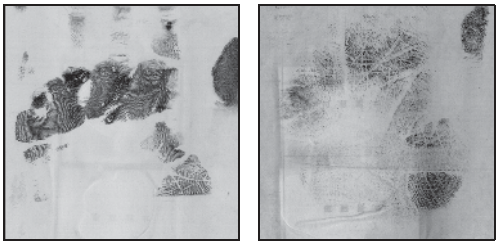

Fig. 15. Two palmprints not successfully registered by the registration algorithm.

As for accuracy, 44 palmprints are not successfully registered, which is 0.3 percent of all the palmprints within the database. All the failure cases are due to improper impression or bad image quality. Two of the failed palmprints are shown in Fig. 15. Currently, we do not have an automatic method to determine whether the registration is correct or not. So, these 44 palmprints also go through the cascade filtering and matching.

4.2.2 Segment-Based Matching and Fusion

The segment-based matching and fusion algorithm comprises the advantages of being robust to skin distortion and making better use of varying discrimination of different palmprint regions. To verify the above advantages, we design three matching algorithms with different combinations of matching and scoring methods. In the first system, palmprints are aligned with global rigid transformations and feature similarity scores are calculated at global level as in [21]. The derived similarity scores are fused by a naive Bayesian with GMM. In the second system, palmprints are aligned at segment level, while feature similarity scores are still calculated globally and fused by a naive Bayesian. In the third system, palmprints are aligned and similarity scores are calculated at the segment level. The performance of these three matching algorithms in full-to-full and partial-to-full matching experiments are shown in Figs. 16. The experiment settings are the same as in Section 4.3.

It can be seen from Fig. 16a that aligning at segment level can greatly improve the performance of matching full palmprints, for which distortion is a serious problem. The results of aligning the palmprints in Fig. 2 at global level and at segment level are shown in Fig. 17. It can be seen that aligning at segment level can effectively deal with the serious distortion. In partial-to-full matching, the system calculating and fusing similarity scores at segment level achieves higher accuracy than the system performs the operations at global level, as shown in Fig. 16b.

4.2.3 Cascade Filtering

The cascade filter is trained on the training set of THUPALMLAB. The maximum number of segments to use, N_{max}, and the desired TRR are set as 2 and 20 percent, respectively. The constructed cascade filter and its performance are shown in Fig. 18. The first filter uses the segment of C2, which corresponds to the region with outstanding discrimination power (see Fig. 7). By comparing one segment, this filter can reject up to 55.7 percent nonmated

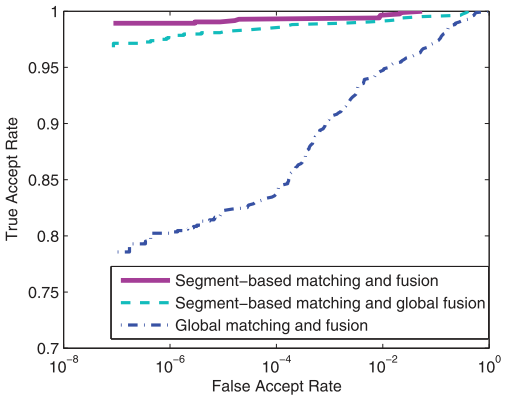

(a)

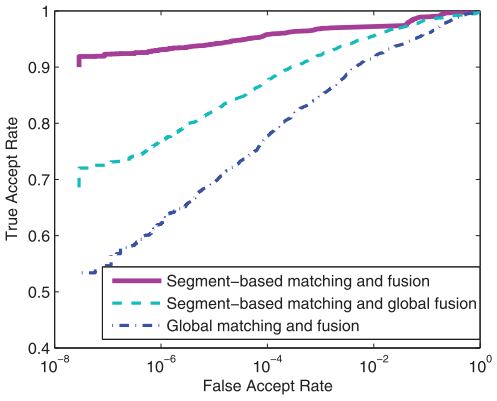

(b)

Fig. 16. ROC curves of three matching and fusion methods: (a) matching 840 full palmprints against the gallery set of 13,736 palmprints, (b) matching 2,520 partial palmprints against the same gallery set.

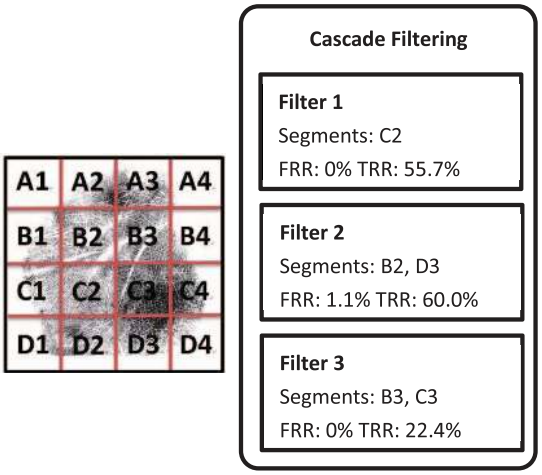

Fig. 18. Constructed cascade filter and its performance in filtering the matchings of 840 full palmprints against the gallery set of 13,736 palmprints.

gallery palmprints while retaining all the mated gallery palmprints. The second filter uses the segment combination of B2 and D3, and 60.0 percent of the remained nonmated gallery palmprints can be rejected. But 1.1 percent of the mated gallery palmprints are also rejected. The third filter uses the segment combination of B3 and C3, resulting in a TRR of 22.4 percent and a FRR of 0 percent. As a whole, the constructed cascade filter achieves a TRR of 86.3 percent when the FRR is 1.1 percent. It can effectively reject the nonmated gallery palmprints by just comparing a small region of the palmprints.

The acceleration gained by cascade filtering is significant. Without cascade filtering, the segment-based matching and fusion algorithm takes about 151 ms to match an impostor matching of full palmprints. When the cascade filtering is performed, the time is reduced to 39 ms, resulting in an average acceleration rate of about 3.9.

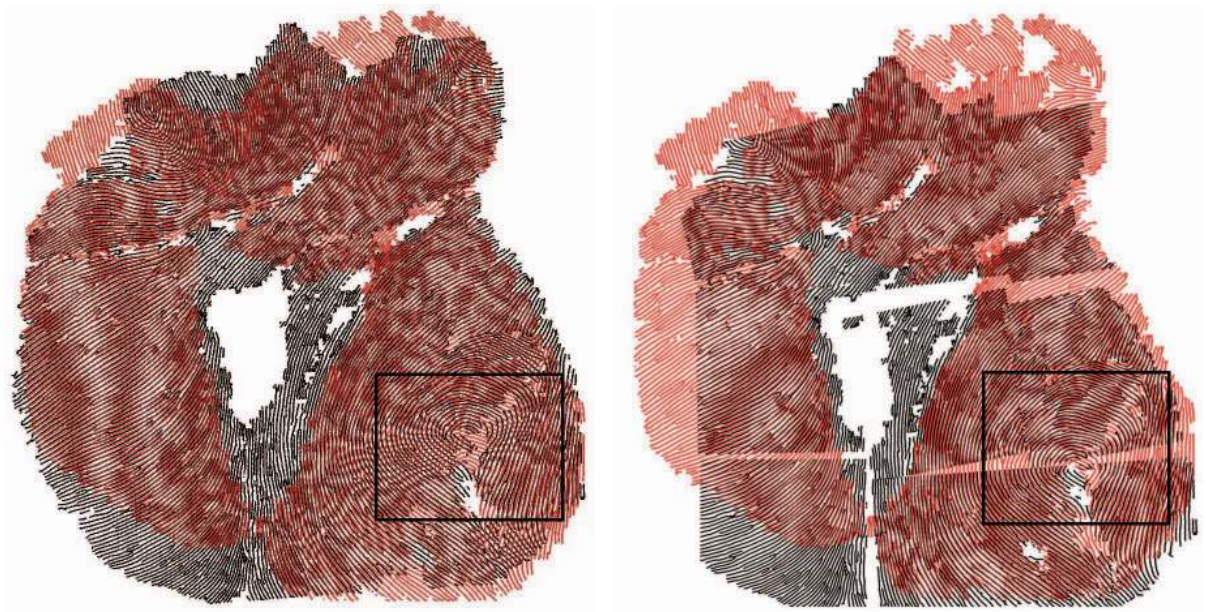

(a) (b)

Fig. 17. Aligning the palmprints in Fig. 2 at different levels: (a) global level, (b) segment level.

In our experiment, when cascade filter is performed, the TAR of the proposed matching algorithm is about 97.9 percent when the FAR is set as 2×10^{-7}, which is 1.1 percent lower than the TAR of the algorithm without cascade filtering.

4.3 Overall Performance

The proposed matching algorithm was compared to the algorithms in [21] and [20] on the THUPALMLAB. The same feature extraction algorithm in [21] was used for all three matching algorithms. Both full-to-full palmprint matching and partial-to-full palmprint matching experiments were conducted. In these experiments, we used the full palmprints from 40 palms in the multiimpression subset as the training set to estimate the PDFs in (9). The first impressions of the rest 120 palms in the multi-impression subset are combined with the uni-impression subset to form the gallery set of 13,736 palmprint images. The same galley set is used in both experiments. In the full palmprint matching experiment, the remaining seven impressions of each of the 120 palms in the multi-impression subset are searched against the gallery set. In the partial palmprint matching experiment, the 21 partial impressions of each of the 120 palms are searched against the gallery set. When matching partial to full prints, the cascade filter is not used because the partial prints are very incomplete.

The performance is shown in both identification Receiver Operating Characteristic (ROC) curves [47] and verification ROC curves. Verification ROC curve is routinely reported for the convenience of comparison, while identification ROC curve measures the performance of the identification system. The identification system operates as follows: Given a query print, the system returns the gallery print whose similarity with the query is larger than the predefined threshold and is the largest one in all gallery prints. If there is no gallery print whose similarity is larger than the threshold, no gallery print is returned. An identification system may make two kinds of error: false negative identification and false positive identification. When the mate of the query is contained in the database but not returned by the system, a false negative identification occurs. When the database does not contain the mate of a query, but the system returns a gallery print, a false positive identification occurs. The false negative identification rate (FNIR) can be measured by performing a number of query whose mate is contained in the database and the false positive identification rate (FPIR) can be measured by performing a number of query which does not have a mate in the database. Since, in our case, each query print has a mate in the database, the FPIR is obtained by setting the similarity with the mate as the lowest value. Another frequently used indicator, true positive identification rate (TPIR), is equal to 1-FNIR. By changing the similarity threshold, we can obtain a set of TPIRs and FPIRs and plot the identification ROC curve.

The identification and verification ROC curves of the full palmprint matching experiment are shown in Fig. 19. In the identification ROC curves, the TPIR of the proposed algorithm is about 97.9 percent when the FPIR is set as 2×10^{-3}, and it is about 17 and 43 percent higher than the algorithms in [21] and [20], respectively. In the verification

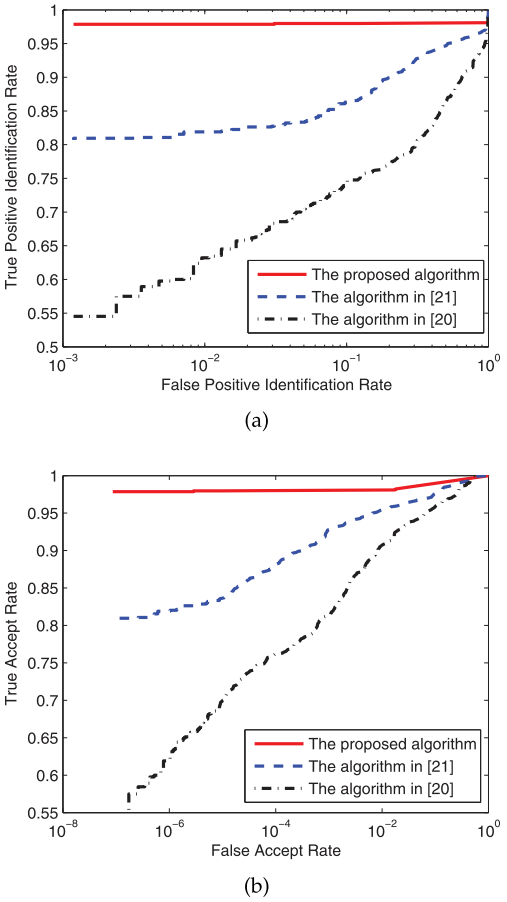

Fig. 19. Identification ROC and verification ROC curves of the proposed algorithm, the algorithms in [21] and [20] in matching 840 full palmprints against the gallery set of 13,736 palmprints: (a) identification ROC curves, (b) verification ROC curves.

ROC curves, the TAR of the proposed algorithm is about 97.9 percent when the FAR is set at 2×10^{-7}, which is about 17 percent higher than the algorithm in [21] and 40 percent higher than the algorithm in [20].

The performance of partial-to-full palmprint matching systems are shown in Fig. 20. According to the identification ROC curves, a TPIR of about 91.9 percent is achieved by the proposed algorithm when the FPIR is set as 5×10^{-4}, about 34 and 65 percent higher than the algorithms in [21] and [20], respectively. According to the verification ROC curves, the TAR of the proposed algorithm is 91.9 percent when the FAR is 3×10^{-8}, 34 and 65 percent higher than the TARs of the algorithms in [21] and [20], respectively. The performance improvement for the partial-to-full matching system is more significant than that for the full palmprint matching system. That is because the influence of varying discrimination power of different palmprint regions is stronger for partial prints, as shown in Section 4.2.2.

To facilitate comparison with other algorithms, we also report the performance on the public multi-mpression subset of THUPLAMLAB, containing 1,280 palmprints from 160 different palms. Since the first 40 palms have been used in the statistical study, the impressions from the left 120 palms are compared against each other in the testing stage. So, 3,360 genuine matchings and 456,960 impostor matchings are generated to measure the performance. Since the gallery size

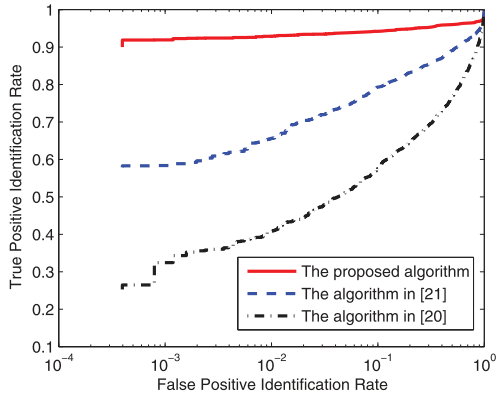

(a)

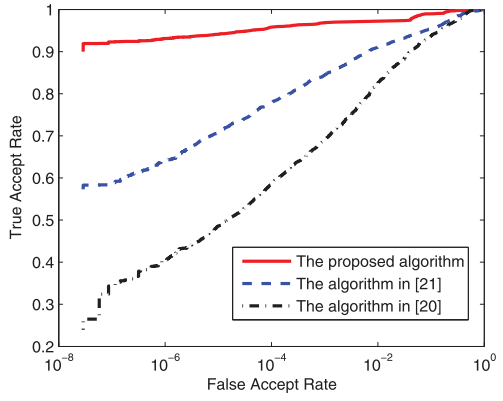

(b)

Fig. 20. Identification ROC and verification ROC curves of the proposed algorithm, the algorithms in [21] and [20] in matching 2,520 partial palmprints against the gallery set of 13,736 palmprints: (a) identification ROC curves, (b) verification ROC curves.

(120) is very small, the performances of the proposed algorithm and the algorithms in [21], [20] are shown as the verification ROC curves in Fig. 21. Besides, we have made our algorithm publicly available on the website of http://ivg.au.tsinghua.edu.cn so that other researchers can test it on other palmprint data sets.

The computational costs of different algorithms are measured on a PC with Intel 2.4 GHz CPU and Windows

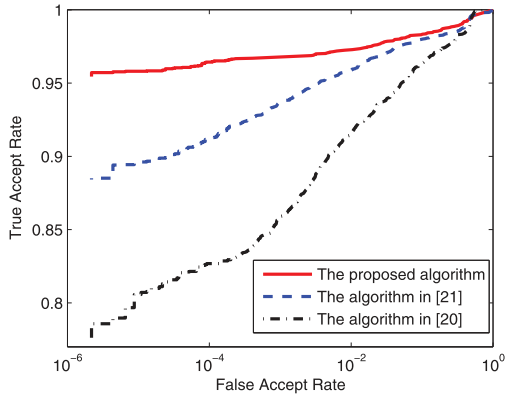

Fig. 21. Verification ROC curves of the proposed algorithm and the algorithms in [21], [20] on the publicly available multi-impression subset of THUPALMLAB.

TABLE 4
Computational Costs of Different Algorithms

Algorithm	Full-to-full matching time (ms)		Partial-to-full matching time (ms)	
	Genuine	Impostor	Genuine	Impostor
Proposed algorithm	161	39	62	57
Algorithm in [21]	5,364	5,158	2,763	2,678
Algorithm in [20]	2,019	1,906	657	623

XP operating system. The feature extraction algorithm in [20] is used for all three matchers, which takes about 55 s for processing a full palmprint. The matching time of different algorithms is shown in Table 4. The cascade filtering is not used for partial-to-full matching, so the speed of the proposed algorithm in partial-to-full matching is slower than that in the full-to-full matching. It should be noted that the proposed algorithm just uses a simple GHT-based minutiae matching algorithm to align palmprints, which is the same as in [21]. The experimental results show that the proposed algorithm improved the speed of the original matching algorithm in [21] by a factor of 132 for full-to-full impostor matching, which consumes most of the computational resources in large identification systems. Note that the acceleration is not only effective for GHT-based minutiae matching algorithm but also for other matching algorithms as well, including other minutiae-based methods [48], [49], [50], texture-based methods [24], [51], image-based methods [38], and so on.

5 Conclusion and Future Work

In recent 10 years, a number of palmprint recognition algorithms have been proposed and most of these algorithms are based on crease features extracted from low-resolution contactless palmprints. However, crease-based palmprint recognition has not been successfully used for large-scale person identification applications because of some inherent limitations. Ridge features in palmprints are proven unique and persistent and identification-based ridge features is accepted in courts of law. Recently, a few ridge-based palmprint recognition systems have been proposed. Although there is some novelty in the feature extraction algorithms, the matching algorithms of these systems are basically adapted from fingerprint matching. Thus, the accuracy of these systems is limited despite heavy computational cost. Motivated by the matching strategies of human palmprint experts, we quantitatively analyzed the statistics of palmprint characteristics and proposed a novel palmprint matching algorithm based on the obtained statistics which achieves higher accuracy as well as lower computational cost than the previous systems. The main contributions include:

1. A quantitative statistical study on palmprints is conducted to guide the design of a robust and efficient 1:N palmprint matching system.
2. A segment-based palmprint matching and fusion algorithm is proposed to deal with distortion and

varying discrimination power of different palmprint features and regions.

3. An orientation field-based registration algorithm and a cascade filter is designed to reduce the computational complexity in 1:N palmprint matching.

The proposed algorithm may also provide assistance for the low-resolution palmprint recognition [5]. The segment-based matching and fusion provides a strategy to deal with distortion and varying discrimination power of different regions for palmprint matching, while the cascade filtering idea may also be useful for acceleration.

The current registration algorithm is designed for registering full palmprints. But the palmprint experts can determine the location of a small latent palmprints based on certain clues, including the latent shape, some fine orientation field and crease features [25]. How to extend the current registration algorithm to partial and latent palmprints is an interesting but challenging problem. The registration algorithm needs to not only estimate the best spatial transformation but also output a confidence value associated with the transformation. Large law enforcement databases can contain as many as millions of palmprint images. While the current matcher is already significantly faster than existing matchers, its efficiency still requires large improvement.

ACKNOWLEDGMENTS

The authors would like to thank Abhishek Nagar for his help in revising this paper. This work was supported by the National Natural Science Foundation of China under Grants 61020106004, 60875017, 61005023, 61021063, and by the National 863 Hi-Tech Development Program of China under Grant 2008AA01Z123.

REFERENCES

[1] D.R. Ashbaugh, *Quantitative-Qualitative Friction Ridge Analysis: An Introduction to Basic and Advanced Ridgeology.* CRC Press, 1999.

[2] M. Kücken and A. Newell, "Fingerprint Formation," *J. Theoretical Biology,* vol. 235, no. 1, pp. 71-83, 2005.

[3] H. Cummins and M. Midlo, *Finger Prints, Palms and Soles: An Introduction to Dermatoglyphics.* Dover Publications, 1961.

[4] W. Li, D. Zhang, and Z. Xu, "Palmprint Identification by Fourier Transform," *Int'l J. Pattern Recognition and Artificial Intelligence,* vol. 16, no. 4, pp. 417-432, 2002.

[5] D. Zhang, W.K. Kong, J. You, and M. Wong, "Online Palmprint Identification," *IEEE Trans. Pattern Analysis and Machine Intelligence,* vol. 25, no. 9, pp. 1041-1050, Sept. 2003.

[6] W. Kong, D. Zhang, and W. Li, "Palmprint Feature Extraction Using 2-D Gabor Filters," *Pattern Recognition,* vol. 36, no. 10, pp. 2339-2347, 2003.

[7] A. Kong and D. Zhang, "Competitive Coding Scheme for Palmprint Verification," *Proc. 17th Int'l Conf. Pattern Recognition,* vol. 1, 2004.

[8] A. Kong, D. Zhang, and M. Kamel, "Palmprint Identification Using Feature-Level Fusion," *Pattern Recognition,* vol. 39, no. 3, pp. 478-487, 2006.

[9] A. Kumar and D. Zhang, "Personal Recognition Using Hand Shape and Texture," *IEEE Trans. Image Processing,* vol. 15, no. 8, pp. 2454-2461, Aug. 2006.

[10] D. Huang, W. Jia, and D. Zhang, "Palmprint Verification Based on Principal Lines," *Pattern Recognition,* vol. 41, no. 4, pp. 1316-1328, 2008.

[11] W. Jia, D. Huang, and D. Zhang, "Palmprint Verification Based on Robust Line Orientation Code," *Pattern Recognition,* vol. 41, no. 5, pp. 1521-1530, 2008.

[12] W. Shu and D. Zhang, "Automated Personal Identification by Palmprint," *Optical Eng.,* vol. 37, no. 8, pp. 2359-2362, 1998.

[13] D. Zhang and W. Shu, "Two Novel Characteristics in Palmprint Verification: Datum Point Invariance and Line Feature Matching," *Pattern Recognition,* vol. 32, no. 4, pp. 691-702, 1999.

[14] N. Duta, A.K. Jain, and K. Mardia, "Matching of Palmprints," *Pattern Recognition Letters,* vol. 23, no. 4, pp. 477-486, 2002.

[15] J. You, W. Li, and D. Zhang, "Hierarchical Palmprint Identification via Multiple Feature Extraction," *Pattern Recognition,* vol. 35, no. 4, pp. 847-859, 2002.

[16] Z. Sun, T. Tan, Y. Wang, and S. Li, "Ordinal Palmprint Representation for Personal Identification," *Proc. IEEE Int'l Conf. Computer Vision and Pattern Recognition,* vol. 1, pp. 279-284, 2005.

[17] F. Yue, W. Zuo, D. Zhang, and K. Wang, "Orientation Selection Using Modified FCM for Competitive-Based Palmprint Recognition," *Pattern Recognition,* vol. 42, no. 11, pp. 2841-2849, 2009.

[18] A. Kumar, "Incorporating Cohort Information for Reliable Palmprint Authentication," *Proc. Indian Conf. Computer Vision, Graphics and Image Processing,* pp. 583-590, 2008.

[19] "Data Format for the Interchange of Fingerprint Facial, & Other Biometric Information," ANSI/NIST-ITL, 1-2007, http://www.nist.gov/customcf/get_pdf.cfm?pub_id=51174. 2012.

[20] A.K. Jain and J. Feng, "Latent Palmprint Matching," *IEEE Trans. Pattern Analysis and Machine Intelligence,* vol. 31, no. 6, pp. 1032-1047, June 2009.

[21] J. Dai and J. Zhou, "Multifeature-Based High-Resolution Palmprint Recognition," *IEEE Trans. Pattern Analysis and Machine Intelligence,* vol. 33, no. 5, pp. 945-957, May 2011.

[22] Neurotechnology Inc., VeriFinger, http://www.neurotechnology.com, 2012.

[23] N. Ratha, K. Karu, S. Chen, and A. Jain, "A Real-Time Matching System for Large Fingerprint Databases," *IEEE Trans. Pattern Analysis and Machine Intelligence,* vol. 18, no. 8, pp. 799-813, Aug. 1996.

[24] J. Feng, "Combining Minutiae Descriptors for Fingerprint Matching," *Pattern Recognition,* vol. 41, no. 1, pp. 342-352, 2008.

[25] Ron Smith and Associates, Inc. "Demystifying Palm Prints," http://www.ronsmithandassociates.com/, 2012.

[26] "Directional Statistics—Wikipedia, the Free Encyclopedia," Wikipedia, http://en.wikipedia.org/wiki/Directionalstatistics, 2011.

[27] D. Wan and J. Zhou, "Fingerprint Recognition Using Model-Based Density Map," *IEEE Trans. Image Processing,* vol. 15, no. 6, pp. 1690-1696, June 2006.

[28] "Hand—Wikipedia, the Free Encyclopedia," Wikipedia, http://en.wikipedia.org/wiki/Hand. 2011.

[29] G. Brunelli, "Stability of the First Carpometacarpal Joint," *Finger Bone and Joint Injuries,* pp. 167-174, Taylor & Francis, 1999.

[30] PolyU Palmprint Database, http://www.comp.polyu.edu.hk/biometrics/, 2012.

[31] K. Bowyer, K. Hollingsworth, and P. Flynn, "Image Understanding for Iris Biometrics: A Survey," *Computer Vision and Image Understanding,* vol. 110, no. 2, pp. 281-307, 2008.

[32] A. Martínez, "Recognizing Imprecisely Localized, Partially Occluded, and Expression Variant Faces from a Single Sample per Class," *IEEE Trans. Pattern Analysis and Machine Intelligence,* vol. 26, no. 6, pp. 748-763, June 2002.

[33] C.C. Han, H.L. Cheng, C.L. Lin, and K.C. Fan, "Personal Authentication Using Palm-Print Features," *Pattern Recognition,* vol. 36, no. 2, pp. 371-381, 2003.

[34] C. Han, "A hand-Based Personal Authentication Using a Coarse-to-Fine Strategy," *Image and Vision Computing,* vol. 22, no. 11, pp. 909-918, 2004.

[35] H. Dutağaci, B. Sankur, and E. Yörük, "Comparative Analysis of Global Hand Appearance-Based Person Recognition," *J. Electronic Imaging,* vol. 17, pp. 011018/1-011018/19, 2008.

[36] A.K. Jain and N. Duta, "Deformable Matching of Hand Shapes for Verification," *Proc. Int'l Conf. Image Processing,* 1999.

[37] D.H. Ballard, "Generalizing the Hough Transform to Detect Arbitrary Shapes," *Pattern Recognition,* vol. 13, no. 2, pp. 111-122, 1981.

[38] C. Watson, P. Grother, and D. Casasent, "Distortion-Tolerant Filter for Elastic-Distorted Fingerprint Matching," *Proc. SPIE Optical Pattern Recognition,* vol. 4043, pp. 166-174, 2000.

[39] R. Cappelli, D. Maio, and D. Maltoni, "Modelling Plastic Distortion in Fingerprint Images," *Proc. Second Int'l Conf. Advances in Pattern Recognition,* pp. 371-378, 2001.

[40] A. Senior and R. Bolle, "Improved Fingerprint Matching by Distortion Removal," *IEICE Trans. Information and Systems,* vol. 84, no. 7, pp. 825-832, 2001.
[41] A.K. Jain, L. Hong, and R.M. Bolle, "On-Line Fingerprint Verification," *IEEE Trans. Pattern Analysis and Machine Intelligence,* vol. 19, no. 4, pp. 302-314, Apr. 1997.
[42] A.K. Jain and J. Feng, "Latent Fingerprint Matching," *IEEE Trans. Pattern Analysis and Machine Intelligence,* vol. 33, no. 1, pp. 88-100, Jan. 2011.
[43] A. Dempster et al., "Maximum Likelihood from Incomplete Data via the EM Algorithm," *J. Royal Statistical Soc. Series B (Methodological),* vol. 39, no. 1, pp. 1-38, 1977.
[44] P. Viola and M. Jones, "Rapid Object Detection Using a Boosted Cascade of Simple Features," *Proc. IEEE Int'l Conf. Computer Vision and Pattern Recognition,* pp. 511-518, 2001.
[45] P. Viola, M. Jones, and D. Snow, "Detecting Pedestrians Using Patterns of Motion and Appearance," *Int'l J. Computer Vision,* vol. 63, no. 2, pp. 153-161, 2005.
[46] A. Ross, K. Nandakumar, and A. Jain, *Handbook of Multibiometrics.* Springer, 2006.
[47] "Biometric Testing and Statistics," NSTC Subcommittee on Biometrics, http://www.biometricscatalog.org/NSTCSubcommittee. 2006.
[48] X. Jiang and W.Y. Yau, "Fingerprint Minutiae Matching Based on the Local and Global Structures," *Proc. Int'l Conf. Pattern Recognition,* pp. 1038-1041, 2000.
[49] A.K. Jain, A. Ross, and S. Prabhakar, "Fingerprint Matching Using Minutiae and Texture Features," *Proc. Int'l Conf. Image Processing,* pp. 282-285, 2001.
[50] X. Chen, J. Tian, and X. Yang, "A New Algorithm for Distorted Fingerprints Matching Based on Normalized Fuzzy Similarity Measure," *IEEE Trans. Image Processing,* vol. 15, no. 3, pp. 767-776, Mar. 2006.
[51] A.K. Jain, S. Prabhakar, L. Hong, and S. Pankanti, "Filterbank-Based Fingerprint Matching," *IEEE Trans. Image Processing,* vol. 9, no. 5, pp. 846-859, May 2002.

Jifeng Dai received the BS degree from Tsinghua University, Beijing, in 2009 where he is currently working toward the PhD degree in the Department of Automation. His research interests are in pattern recognition and computer vision.

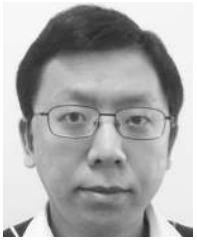

Jianjiang Feng received the BS and PhD degrees from the School of Telecommunication Engineering, Beijing University of Posts and Telecommunications, China, in 2000 and 2007, respectively. He is an assistant professor in the Department of Automation at Tsinghua University, Beijing. From 2008 to 2009, he was a postdoctoral researcher in the Pattern Recognition and Image Processing Laboratory at Michigan State University. His research interests include fingerprint recognition, palmprint recognition, and structural matching. He is a member of the IEEE.

Jie Zhou received the BS and MS degrees from the Department of Mathematics, Nankai University, Tianjin, China, in 1990 and 1992, respectively, and the PhD degree from the Institute of Pattern Recognition and Artificial Intelligence, Huazhong University of Science and Technology (HUST), Wuhan, China, in 1995. From 1995 to 1997, he was a postdoctoral fellow with the Department of Automation, Tsinghua University, Beijing, China. Currently, he is a full professor with the Department of Automation, Tsinghua University. His research area includes pattern recognition, computer vision, and data mining. In recent years, he has authored more than 100 papers in peer-reviewed international journals and conferences. He received the Best Doctoral Thesis Award from HUST in 1995, First Class Science and Technology Progress Award from Ministry of Education (MOE) in 1998, Excellent Teaching Award from Tsinghua University in 2003, and Best Advisor Awards from Tsinghua University in 2004 and 2005, respectively. He was selected as one of outstanding scholars of MOE in 2005. He is an associate editor for the *International Journal of Robotics and Automation* and *Acta Automatica Sinica*. He is a senior member of the IEEE.

▷ **For more information on this or any other computing topic, please visit our Digital Library at** www.computer.org/publications/dlib.